

# Strain Engineering Ferromagnetic-Ferroelectricity in Two-Dimensional Multiferroic $\text{VOCl}_2$ Monolayer

Akshay Mahajan<sup>1,\*</sup> and Somnath Bhowmick<sup>1,†</sup>

<sup>1</sup>*Department of Materials Science and Engineering,  
Indian Institute of Technology, Kanpur, Kanpur 208016, India*  
(Dated: December 22, 2024)

Two-dimensional (2D) magnetoelectric multiferroics are promising multifunctional materials for miniaturized logic and memory devices. Herein, we explore the effectiveness of strain-engineering for tuning the properties of a recently predicted 2D antiferromagnetic-ferroelectric,  $\text{VOCl}_2$  monolayer. Interestingly, we find that magnetic-ordering and electric polarization can be tuned independently using uniaxial tensile strain along different in-plane lattice vectors. A 4% tensile strain along lattice vector  $b$  induces a transition from an antiferromagnetic (AFM) ground state with an out-of-plane magnetization to a ferromagnetic (FM) ground state with in-plane magnetization. On the other hand, tensile strain along lattice vector  $a$  enhances spontaneous electric polarization, without affecting the magnetic ordering. The monolayers remain dynamically stable under tensile strain, which further helps to raise the Curie temperature of ferromagnetism, as well as ferroelectricity. Such a strain-tunable multiferroic material holds great promises for future generation nanoelectronic devices.

## I. INTRODUCTION

Magnetoelectric multiferroics<sup>1–3</sup> have fascinated materials scientists and engineers for the last two decades with their rich fundamental physics of combining electronic and magnetic properties and its applications for nanoelectronics. This unique characteristic of combining electric and magnetic ferroic properties makes them potential multifunctional materials for designing devices where a single device component can perform more than one task. This quality is especially desirable for the miniaturization of devices<sup>4</sup>. Among these multiferroics, particular significance is given to ferromagnetic-ferroelectric (FM-FE) materials, which can be used for new device architectures based on four logic states<sup>5,6</sup>.

Realization of enhanced multiferroic properties, e.g., enlarged polarization in thin-films of three-dimensional (3D) multiferroics, have further stimulated multiferroic research for miniaturized non-volatile logic and memory devices<sup>7–10</sup>. However, these thin films have limitations due to the requirement of a critical thickness for sustaining the ferroelectric (FE) state due to the effects of surface, depolarizing electrostatic field, and electron screening<sup>11–16</sup>. Therefore, for the advancement of nanoelectronics, new low-dimensional multiferroics are required. Recently, using first-principles simulations, various two-dimensional (2D) magnetic<sup>17–21</sup>, ferroelectric<sup>22–24</sup>, and multiferroic materials have been discovered<sup>25</sup>. Several approaches, including intercalation<sup>26,27</sup>, doping<sup>28</sup>, and defect engineering<sup>29</sup>, have been used to design 2D FE ferromagnetism. Various other multiferroics have also been discovered<sup>30–34</sup>; most of them belonging to the type-I<sup>2</sup> category, where ferroelectricity and magnetism have independent origins with high polarization values but relatively weak magnetoelectric coupling. The type-II<sup>2</sup> multiferroics, where the magnetic arrangements induce ferroelectricity and thus results in strong magnetoelectric coupling with smaller

polarization values, are quite rare. To the best of our knowledge, MXene  $\text{Hf}_2\text{VC}_2\text{F}_2$  monolayer<sup>35</sup> is the only type-II multiferroic, among 2D materials.

Single-phase one-cation type-I multiferroic monolayers  $\text{VOX}_2$  ( $X = \text{Cl}, \text{Br}, \text{I}$ ) family<sup>36,37</sup> is an interesting new addition to the ever-increasing list of 2D multiferroics. These monolayers have been demonstrated to violate the  $d^0$  rule in multiferroics<sup>37,38</sup>. Generally, it has been observed that the partial occupancy of d-orbitals of transition metal cations, which is essential for the origin of magnetism, suppresses the occurrence of ferroelectricity. However, in  $\text{VOX}_2$  monolayers,  $d^0$  rule gets violated since the partially occupied d-orbital lies in a plane perpendicular to the ferroelectric polarization and such a configuration even helps to enhance the electric polarization in these monolayers.<sup>37</sup>

Among  $\text{VOX}_2$  family of 2D multiferroics,  $\text{VOCl}_2$  monolayer has been predicted as an easily exfoliable 2D antiferromagnetic-ferroelectric (AFM-FE) with an in-plane spontaneous electric polarization and an out-of-plane magnetization<sup>36</sup>. In this work, using first-principle calculations, we demonstrate that the magnetic ordering in  $\text{VOCl}_2$  can be tuned via strain-engineering, along with the enhancement of electric polarization. The transition from AFM-FE to FM-FE state takes place at around 4% in-plane biaxial tensile strain, which also leads to significant enhancement ( $\sim 14\%$ ) of electric polarization. We further establish that, the uniaxial strain along the in-plane lattice vector  $b$  and  $a$  is separately responsible for the change in ground-state magnetic ordering and increase in the FE polarization, respectively. Increasing energy barrier for polarization switching, as well as an enhancement of magnetic exchange coupling parameter predicts both ferroelectric and ferromagnetic Curie temperature to increase with increasing tensile strain. The dependence of the ferroelectric switching energy barrier on the ground state magnetic ordering also suggests some kind of magnetoelectric coupling. A comparison of mag-

netocrystalline anisotropy energies also reveal a  $90^\circ$  rotation of magnetization direction, associated with the transition from the state of AFM-FE (out of plane) to FM-FE (in plane).

Scope of tuning a 2D ferroelectric material (having in-plane electric polarization) via applying strain along the polar axis has recently been explored in several studies.<sup>39,40</sup> However, to the best of our knowledge, this is the first report on strain engineering of a 2D multiferroic material, showing that different ferroic properties can be *independently* controlled via applying strain along different in plane crystallographic directions, which makes  $\text{VOCl}_2$  a very promising material for next generation nanoelectronic devices.

## II. COMPUTATIONAL DETAILS

All first-principles calculations are performed within the framework of density functional theory (DFT) using a plane-wave basis set, as implemented in the VASP suite of codes.<sup>41–43</sup> Projector augmented wave (PAW)<sup>44,45</sup> pseudopotentials are used in which exchange and correlation effects are treated within a generalized gradient approximation (GGA) scheme, developed by Perdew-Burke-Ernzerhof (PBE).<sup>46</sup> For all structural relaxation and electronic structure calculations, except the phonon spectra calculations, vdW-DF2<sup>47–50</sup> non-local correlation functional is used to account for dispersion interactions. For DFT+U based calculations, effective U values are added according to the method proposed by Dudarev *et al.*<sup>51</sup> 2D  $\text{VOCl}_2$  monolayer is exfoliated from its 3D parent, which is retrieved from the Inorganic Crystal Structure Database (ICSD)<sup>52</sup> with ICSD number 24380. All calculations are done for a  $2 \times 2 \times 1$  supercell of  $\text{VOCl}_2$  unit cell to consider different magnetic orderings. A vacuum layer of 20 Å is added along  $c$ -axis ( $z$ -direction) to avoid the spurious interaction between the monolayer and its periodic images. An energy cutoff of 520 eV is used for the plane-wave basis set with a  $k$ -mesh of  $7 \times 7 \times 1$  for the Brillouin zone (BZ) integrations. For structural relaxation, a criterion of 0.001 eV/Å for the Hellman-Feynman forces is used, and optimization of atomic positions and lattice constants are done using a conjugate gradient (CG) algorithm. The phonon spectra are calculated using the linear response method, which utilizes density functional perturbation theory (DFPT), as implemented in Phonopy.<sup>53</sup> The electric polarization is calculated using the Berry phase method.<sup>54,55</sup> The MAE is calculated using the magnetic force theorem.<sup>56–58</sup> Tensile strain along different lattice parameters is defined as  $\varepsilon = (a - a_0)/a_0 = (b - b_0)/b_0$ , where  $a$ ,  $b$  are in-plane lattice parameters and  $a_0$ ,  $b_0$  are the equilibrium lattice constants.

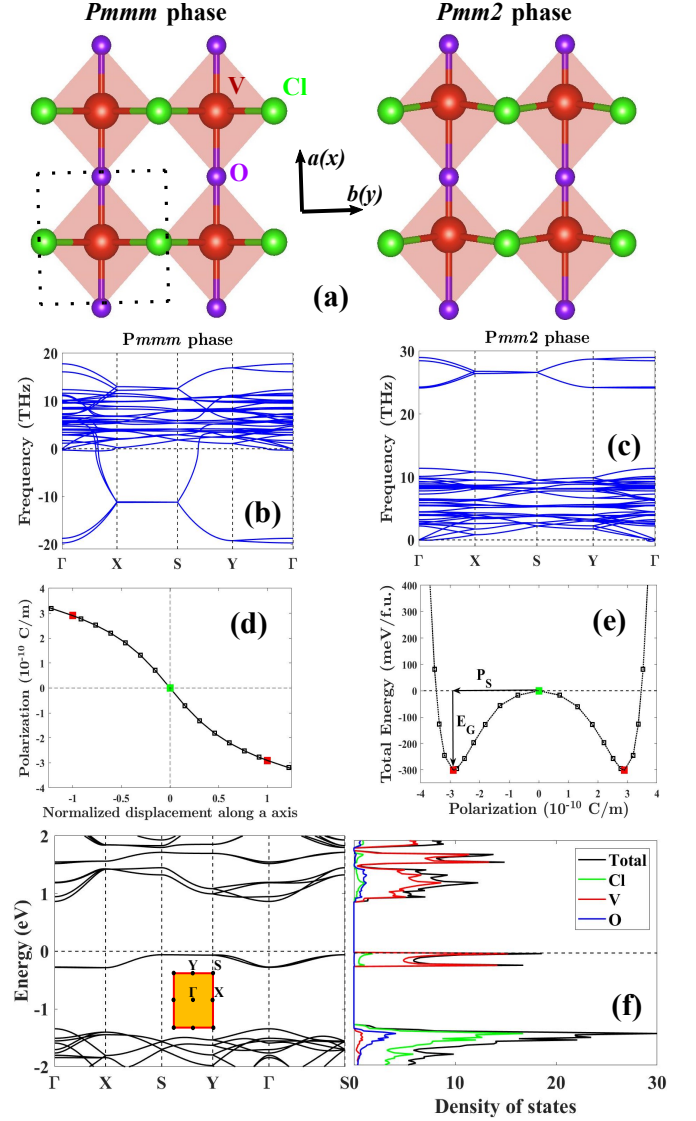


FIG. 1. (a) Top views of the high ( $Pmmm$ ) and low-symmetry ( $Pmm2$ )  $\text{VOCl}_2$  monolayers. Black dotted rectangle denotes the primitive cell (containing an octahedron). Phonon spectra of the (b)  $Pmmm$  and (c)  $Pmm2$  phases, respectively. (d) Calculated total polarization as a function of normalized displacement along the adiabatic path. (e) Double-well potential of  $\text{VOCl}_2$  monolayer. Green and red squares in (d) and (e) represents PE ( $Pmmm$ ) and FE ( $Pmm2$ ) phases, respectively. (f) Electronic band structure (left) and orbital resolved density of states (right) of monolayer  $\text{VOCl}_2$  with AFM3 ground state magnetic ordering. High-symmetry points in the first Brillouin zone are also shown in the inset.

## III. RESULTS AND DISCUSSIONS

The top view of the crystal structure of the  $\text{VOCl}_2$  monolayer is illustrated in Figure 1(a). Among the two phases, namely the paraelectric (PE)  $Pmmm$  and FE  $Pmm2$ , the V ion along the V-O chain (parallel to the polar axis or  $a$ -axis) is displaced in the latter. The V ion displacement lifts the inversion center present in the

PE phase within the  $\text{VOCl}_2$  octahedra [Figure S1 of Supplemental Material<sup>59</sup>], leading to a spontaneous polarization. The phonon spectra of PE and FE phases [Figure 1(b) and 1(c)] reveals the presence of soft optical modes in the former (arising because of the displacement of the V ion); suggesting spontaneous symmetry breaking below the Curie temperature, causing the transition from the high-symmetry PE phase to the low-symmetry FE phase.<sup>60</sup> Figure 1(d) shows the variation of total polarization of the  $\text{VOCl}_2$  monolayer as a function of the V ion displacement along the polar axis ( $a$ -axis), which confirms the direct proportionality of the electric polarization to the amount of V ion's displacement from the inversion center. The polarization-displacement curve also displays how the sign of the polarization depends on the direction of V ion displacement along the polar axis. The characteristic marker of spontaneous electric polarization, the double-well potential, is also plotted in Figure 1(e). From the double-well potential, spontaneous electric polarization ( $P_S$ ) value of  $2.9 \times 10^{-10}$  C/m and a potential barrier ( $E_G$ ) of 301 meV per cation [or per formula unit (f.u.)] is determined, which are similar to the values predicted in earlier works.<sup>36,37</sup> According to our first-principles calculations, among the four magnetic states considered in this work [Figure S2<sup>59</sup>], the ground-state magnetic ordering is AFM3. Figure 1(f) shows the electronic band structure of the AFM3  $\text{VOCl}_2$  monolayer, along with orbital projected density of states (PDOS) plot. Evidently,  $\text{VOCl}_2$  monolayer has an indirect band gap of about 0.92 eV with valence band and conduction band nearest to the Fermi level being predominately contributed by V atoms.

To understand the effect of strain on the magnetic (ferroelectric) properties of  $\text{VOCl}_2$  monolayer, the energy difference between the FM and remaining three AFM states (the polar displacement in the monolayer) is calculated for each strain percent, as illustrated in Figure 2. Here, the polar displacement is defined as the difference between the fractional coordinates of V ion along the polar axis ( $a$ -axis) in the PE and FE state. As shown in Figure 2(a), the energy difference among different magnetic states does not change with lattice parameter  $a$  and as a result, AFM3 remains the lowest energy magnetic state. On the other hand, as lattice parameter  $b$  is increased, FM becomes the lowest energy magnetic state for 4% and higher strain percent [Figure 2(b)]. Interestingly, an in-plane biaxial tensile strain results a similar magnetic phase transition [Figure 2(c)] around same value of applied strain. This clearly suggests that, ground-state magnetic ordering for the  $\text{VOCl}_2$  monolayer depends *exclusively* on lattice parameter  $b$ , while lattice parameter  $a$  has no effect on the magnetic ground state.

The polar displacement, on the other hand, increases monotonically and decreases slightly with increasing lattice parameter  $a$  [Figure 2(d)] and  $b$  [Figure 2(e)], respectively, irrespective of the magnetic ordering. Since polar displacement is directly related to the spontaneous electric polarization and the primary source for its ori-

gin, we find that the spontaneous electric polarization also increases significantly and decreases slightly with tensile strain along the  $a$  and  $b$  direction, respectively [Figure S3<sup>59</sup>]. Thus, the ferroelectric property can be enhanced either via strain-engineering along the polar axis, or via in-plane biaxial tensile strain as well [Figure 2(f)]. The dynamical stability of the FM-FE  $\text{VOCl}_2$  monolayers obtained from in-plane biaxial tensile strain is verified by the phonon spectra, where no imaginary-frequency modes are observed [Figure S4<sup>59</sup>].

So far, our study reveals that, ferroelectric and magnetic properties can be independently controlled via applying strain along the two different in plane crystallographic directions. Therefore, the possibility of engineering both the properties simultaneously via bi-axial strain is explored. As shown in Figure 3(a), spontaneous electric polarization ( $P_S$ ) values increase monotonically for both AFM3 and FM ordering. The similarity in strain dependence arises possibly because, both AFM3 and FM ordering have similar lattice parameters. Nevertheless,  $P_S$  values do depend on magnetic ground state, with AFM3 monolayer having marginally higher values of  $P_S$  than that of FM for each strain percent, which suggests a weak magnetoelectric coupling, similar to that of type-I multiferroics. Since the polar displacement is almost the same for all the magnetic orderings [Figure 2(f)], thus any difference between the electric polarization values of different magnetic orderings must be arising from electronic contribution, rather than the ionic displacement. Increment in the V ion magnetic moment ( $M_V$ ) with increasing tensile strain is also observed in both FE and PE monolayers of AFM3 and FM magnetic state [Figure 3(b)]. FM monolayers are observed to have higher  $M_V$ , than that of AFM3, in both FE and PE monolayers. Note that, rate of increase of  $M_V$  with increasing tensile strain is very small in case of FE monolayers, than compared to PE monolayers, and the latter has slightly higher  $M_V$  values as well. This again suggest that the magnetoelectric coupling present in  $\text{VOCl}_2$  monolayers is rather weak.

To inspect the stability and robustness of ferroelectric state, the configurational energy barriers for polarization reversal in AFM3-FE and FM-FE  $\text{VOCl}_2$  monolayers are determined. Two different polarization switching pathways for the  $\text{VOCl}_2$  monolayers are considered. One pathway (Path-1) goes through the intermediate PE phase, which is the case of characteristic double-well potential shown in Figure 1(e). The second pathway (Path-2) goes through the intermediate antiferroelectric (AFE) phase, which has been predicted in a previous study<sup>36</sup> to be the pathway with the lowest activation barrier. These activation energy barriers are defined as the depth of the double-well potential ( $E_G$ ), in case of Path-1, and the height of the energy peaks in the FE-AFE-FE transformation ( $\Delta E$ ), in case of Path-2, as shown in Figure 1(e) and Figure S5<sup>59</sup>, respectively. A monotonic increment in  $E_G$  values (Path-1) with bi-axial tensile strain for both AFM3 and FM orderings is observed [Figure 3(c)]. For FM monolayers, these values are slightly lower compared

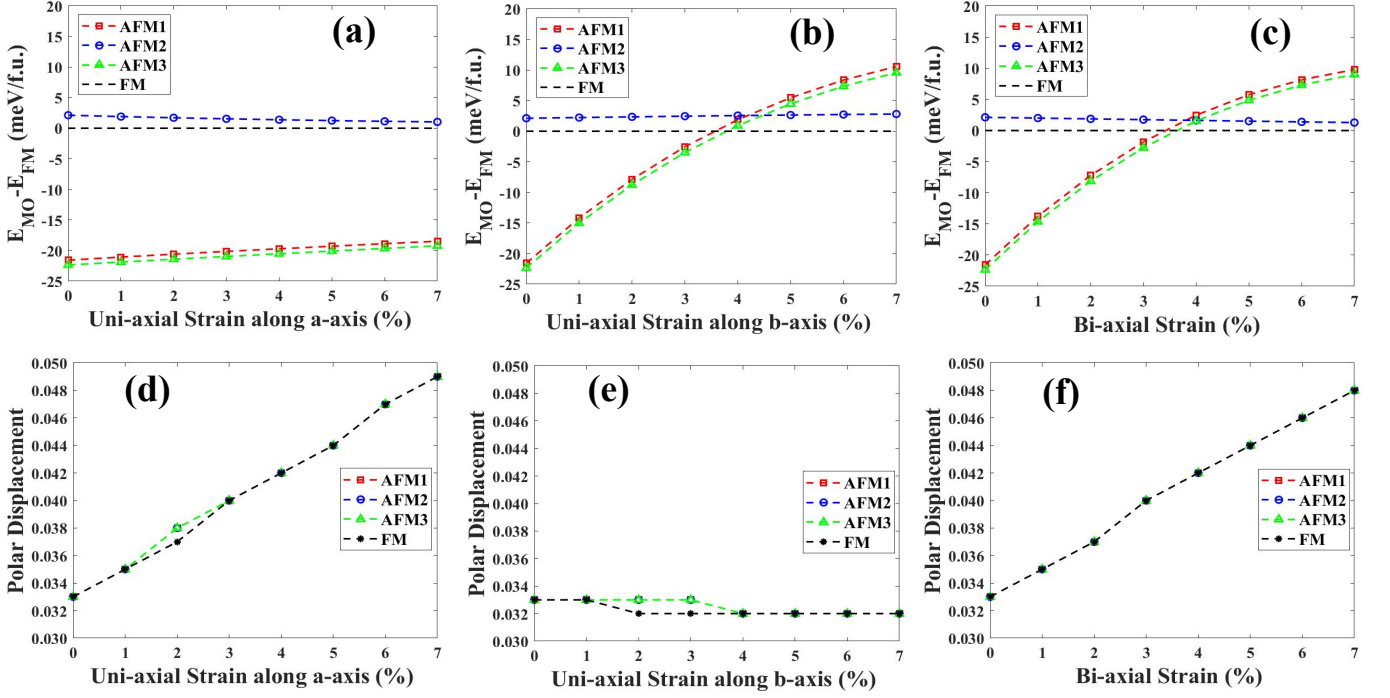


FIG. 2. Variation of energy difference between different magnetic orderings (MO) and FM magnetic ordering [(a), (b), (c)], and dependence of V ion's polar displacement [(d), (e), (f)] in the  $\text{VOCl}_2$  monolayer on the uniaxial strain along  $a$ -axis [(a), (d)], on the uniaxial strain along  $b$ -axis [(b), (e)], and on the in-plane biaxial strain [(c), (f)]. Polar displacement is defined as the difference of the fractional coordinates of V ion along the  $a$ -axis in the PE and FE unit cells.

to those of AFM3 monolayers by 5-14 meV/f.u. and the difference increases with bi-axial tensile strain. A similar trend is observed for  $\Delta E$  values (Path-2) as well. Initially, AFM3 (magnetic ground state) monolayers have higher  $\Delta E$  values (by 21 meV/f.u. at zero strain) than those of FM monolayers. However, as the latter becomes the magnetic ground state for a bi-axial tensile strain of 4% and above,  $\Delta E$  values for the FM monolayer become higher than those of AFM3 monolayers by 2-7 meV/f.u [Figure 3(d) and (e)]. Dependence of  $E_G$  and  $\Delta E$  on magnetic ground state is another evidence of weak magnetoelectric coupling present in  $\text{VOCl}_2$  monolayers.

Our results so far clearly show that the activation energy barrier for electric polarization switching can be tuned via bi-axial strain and it also depends on magnetic order. This is further investigated by applying uniaxial tensile strain along the in-plane lattice vectors, as shown in Figure S6 ( $E_G$  vs. strain) and Figure S7 ( $\Delta E$  vs. strain)<sup>59</sup>. This confirms that the monotonic increase in both  $E_G$  and  $\Delta E$  values are because of the tensile strain along the polar axis ( $a$ -axis). However, the crossover observed in  $\Delta E$  vs. strain plot of AFM3 and FM phase at 4% bi-axial tensile strain [Figure 3(d) and (e)] happens because of the change of  $b$ -lattice parameter [Figure S7].<sup>59</sup>

Since  $E_G$  values are almost twice the  $\Delta E$  values, we conclude that Path-2 [Figure S5] is the one with minimum activation energy, irrespective of the magnitude of strain. Although the AFE phase has energy values close to the FE phase [Figure S5<sup>59</sup>], they are separated by

energy barriers ranging from 151-439 meV/f.u. [Figure 3(d)], which are much larger than the energy of thermal motion at room temperature (25 meV). Thus, these high energy barriers ensures the stability of the FE state.  $E_G$  (ranging from 301-863 meV/f.u. and 296-849 meV/f.u. for AFM3 and FM state, respectively) and  $\Delta E$  (ranging from 151-432 meV/f.u. and 130-439 meV/f.u. for AFM3 and FM state, respectively) values are comparable (or even higher in some cases) to those of typical ferroelectrics such as  $\text{BaTiO}_3$ ,  $\text{PbTiO}_3$ , and  $\text{LiNbO}_3$ ,<sup>61,62</sup> strongly implying the high stability of ferroelectric phase in  $\text{VOCl}_2$  monolayers, which further increases with increasing tensile strain along the polar axis.

To analyze robustness of the magnetic ground state in  $\text{VOCl}_2$  monolayers and how it is affected by strain, we calculate the magnetic exchange coupling parameters, as needed by the following Ising model Hamiltonian,<sup>36</sup>

$$H = H_0 - \sum_{\langle ij \rangle_a} J_a M_i M_j - \sum_{\langle mn \rangle_b} J_b M_m M_n - \sum_{\langle\langle kl \rangle\rangle} J_{ab} M_k M_l, \quad (1)$$

where  $H_0$  is the non-magnetic Hamiltonian;  $M_i$  is the net magnetic moment at site  $i$ ;  $\langle ij \rangle_a$  ( $\langle mn \rangle_b$ ) corresponds to the nearest-neighbor or NN V atoms along the  $a$ -( $b$ )-axis;  $\langle\langle kl \rangle\rangle$  stands for the next-nearest-neighbor or NNN V atoms;  $J_a$  and  $J_b$  are NN magnetic exchange coupling parameters along  $a$ - and  $b$ -directions,



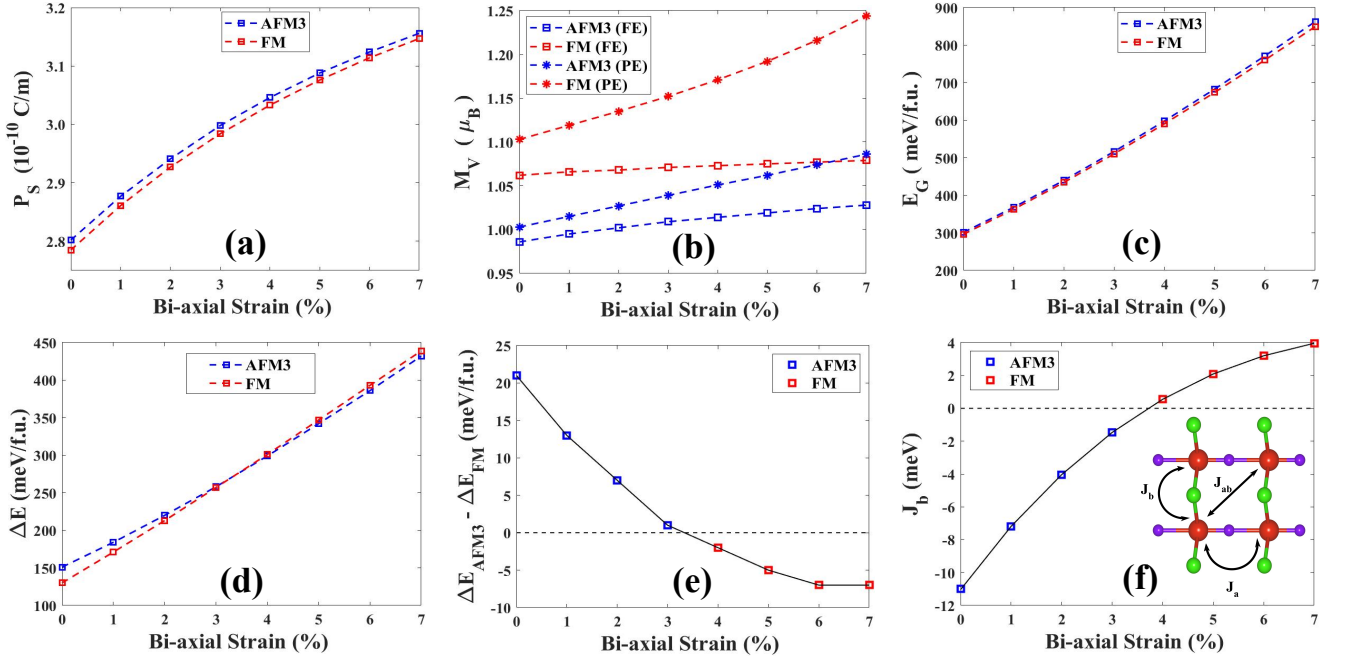


FIG. 3. Influence of the in-plane biaxial strain on the (a) spontaneous electric polarization ( $P_S$ ), (b) V ion's magnetic moment ( $M_V$ ), (c) depth of the double-well potential ( $E_G$ ), and (d) energy barrier ( $\Delta E$ ) for the polarization switching from  $-P_S$  to  $+P_S$  via AFE intermediate phase, for both FM and AFM3 magnetic states. (e) Dependence of the difference between the  $\Delta E$  values for AFM3 and FM magnetic state on in-plane biaxial tensile strain. (f) Change in the nearest-neighbor exchange coupling parameter along b-direction ( $J_b$ ) with biaxial strain. Black dotted line in (e) and (f) represents ground state magnetic order transition from AFM3 to FM.

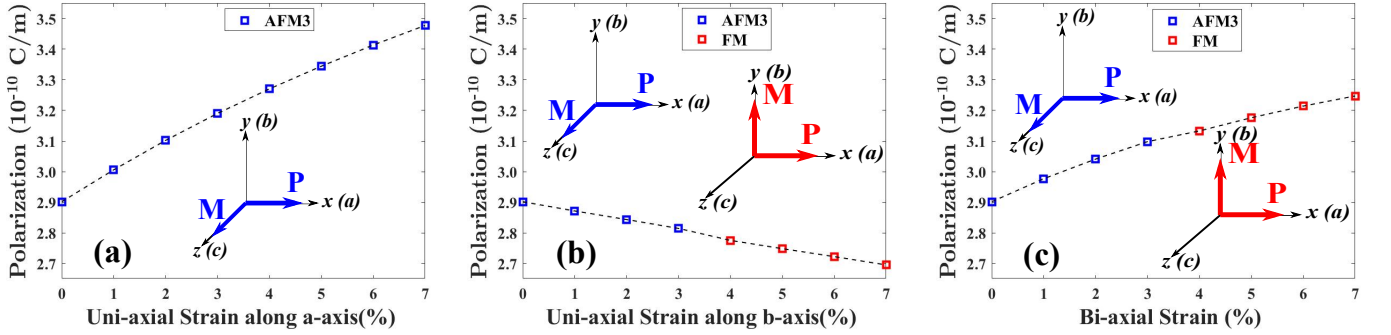


FIG. 4. Variation of spontaneous electric polarization and ground state magnetic ordering in the  $\text{VOCl}_2$  monolayer with (a) uniaxial tensile strain along  $a$ -axis, (b) uniaxial tensile strain along  $b$ -axis, and (c) in-plane biaxial tensile strain. Insets show the direction of magnetic and electric polarization for AFM3 (blue) and FM (red) magnetic ordering. Note the magnetization direction is along  $[001]$  ( $z$ -axis) and  $[010]$  ( $y$ -axis) for AFM3 and FM magnetic ordering, respectively. The color of the squares represents the ground state magnetic ordering at that particular strain percent.

respectively;  $J_{ab}$  is the NNN exchange coupling parameter [see Figure 3(f) inset for schematic representation of exchange coupling parameters]. Using the above Hamiltonian, the total energies for four magnetic orderings can be written as:

$$E_{FM} = E_0 - 4M_{FM}^2(J_a + J_b + 2J_{ab}), \quad (2)$$

$$E_{AFM1} = E_0 - 4M_{AFM1}^2(J_a - J_b - 2J_{ab}), \quad (3)$$

$$E_{AFM2} = E_0 - 4M_{AFM2}^2(-J_a + J_b - 2J_{ab}), \quad (4)$$

$$E_{AFM3} = E_0 - 4M_{AFM3}^2(-J_a - J_b + 2J_{ab}). \quad (5)$$

Here,  $E_0$  is the non-magnetic energy, and  $M_{MO}$  (where  $MO = FM, AFM1, AFM2, AFM3$ ) are magnetic moment values for different magnetic orderings. The above four equations are solved using energy and magnetic moment values calculated from our first-principles calculations to obtain the exchange coupling parameters. As can be seen from Table S1<sup>59</sup>, the exchange coupling parameter along  $b$ -direction,  $J_b$ , is the highest in magnitude among the three coupling parameters for each biaxial and most of the uniaxial strain percent (other than a single exception very close to the magnetic phase transition). Not only  $J_b$

values are higher than the rest, but also it changes much more (including a sign reversal) than compared to  $J_a$  and  $J_{ab}$  with increasing lattice parameter  $b$ . This further corroborates the observation that the magnetic ground state depends *exclusively* on the lattice parameter  $b$  [Figure 2(a)-(c)].

Having established  $J_b$ , which depends on lattice parameter  $b$ , as the dominant exchange coupling parameter, we can now qualitatively predict how the magnetic transition temperature changes with strain. As shown in Figure 3(f), value of  $J_b$  gradually changes from  $-11.04$  to  $3.96$  meV with increasing biaxial tensile strain. The crossover from negative to positive values (near 4% strain) signals a change of magnetic ground state from AMF3 to FM. Since a higher magnitude of the  $J_b$  value can be related to higher stability of magnetic ordering against thermal fluctuations, we can predict from Figure 3(f) that the Néel temperature ( $T_N$ ) for AFM3 ground state ordering will decrease, while the Curie temperature ( $T_C$ ) for FM ground state ordering will increase with biaxial tensile strain. Figure S8 in Supplemental Material<sup>59</sup> further confirms a similar trend for uniaxial strain along  $b$ -axis also.

For 2D materials, long-range magnetic order stabilization requires lifting of the Mermin-Wagner restriction<sup>63</sup>, which is possible by the presence of magnetic anisotropy<sup>64,65</sup>. Therefore, taking spin-orbit coupling (SOC) approximation into account, we evaluate the magnetic anisotropy energy (MAE) values for strained  $\text{VOCl}_2$  monolayers. We consider magnetization along three in-plane directions: [100], [010], [110], and two out-of-plane directions: [001], [111]. From MAE values shown in Table S2 of the Supplemental Material<sup>59</sup>, it is confirmed that the easy axis is along [001] direction and along [010] direction for AFM3 and FM ground state, respectively, both of which are perpendicular to the ferroelectric polarization direction [100]. Therefore, AFM3-FE monolayers show out-of-plane magnetization with in-plane ferroelectricity, while FM-FE monolayers show both in-plane magnetization and ferroelectricity in mutually perpendicular directions. Figure 4 illustrates how polarization and ground-state magnetic ordering change in  $\text{VOCl}_2$  monolayers with increasing in-plane uniaxial and biaxial tensile strain. The insets in Figure 4 also depict the  $90^\circ$  rotation of the magnetization direction with the change in the ground-state magnetic ordering around 4% tensile strain. The spontaneous polarization values ranges from  $2.9 \times 10^{-10}$  to  $3.3 \times 10^{-10}$  C/m for in-plane biaxial tensile strain case, which are comparable to the predicted values for 2D ferroelectric monolayer group-IV monochalcogenides ( $1.51 \times 10^{-10}$  to  $5.06 \times 10^{-10}$  C/m).<sup>12</sup>

To understand the mechanism behind the ground-state magnetic order transition in  $\text{VOCl}_2$  monolayers with tensile strain, we take into account two kinds of exchange interactions among V ions. The first is the direct exchange interaction between the local moments on adjacent V ions [see Figure S10 in Supplemental Material<sup>59</sup>], favoring anti-parallel spin alignment.<sup>37</sup> In case of  $\text{VOCl}_2$

monolayer, neighboring V ions are located closer to each other along the  $b$ -axis (3.459 Å), compared to that of  $a$ -axis (3.815 Å). As a result, orbitals of neighboring V ions overlap by a relatively larger extent along the  $b$ -axis, leading to a strong direct-exchange coupling and a negative  $J_b$  value, which is one order of magnitude larger than that of  $J_a$  and  $J_{ab}$ , both of which have positive sign. However, the change of sign of  $J_b$  at 4% tensile strain along the  $b$ -direction can not be explained by this model.

The second possibility is a halogen or oxygen mediated superexchange interaction between neighboring V ions. Since V-Cl-V (V-O-V) bonds make an angle of  $\sim 90^\circ$  ( $\sim 180^\circ$ ), superexchange interaction is predicted to favor a parallel (antiparallel) spin alignment in neighboring V ions, according to the Goodenough-Kanamori rules.<sup>66-68</sup> The likeliness of anion mediated superexchange interaction is first checked by looking at the orbital-resolved density of states (DOS) plots [Figure S9 in Supplemental Material<sup>59</sup>], which reveal that the valence states closer to the Fermi level arise mainly from out of the plane V- $d_{z^2}$  orbitals and partly from V- $d_{x^2-y^2}$ , as well as Cl-p orbitals. In literature, this predominantly out of the plane (V- $d_{z^2}$ ) nature of the valence states near the Fermi level, which is perpendicular to the polar axis, has been identified as the reason behind violation of the  $d^0$  rule in  $\text{VOCl}_2$ .<sup>37</sup> Because of the overlap of atomic orbitals with energies close to the Fermi level, it is certainly possible to have a superexchange interaction between nearest neighbor V ions, mediated through Cl ions [see Figure S10 in Supplemental Material<sup>59</sup>]. Since O-p levels are located far away from the Fermi energy, O-mediated superexchange mechanism can be ruled out. From Figure S1<sup>59</sup>, it can be seen that V-Cl bonds are along the  $b$ -axis ( $y$ -direction), while the V-O bonds are along the  $a$ -axis ( $x$ -direction). Therefore, the superexchange mechanism, if present, is supposed to be active only along the  $b$ -direction.

Our results suggest that the direct-exchange interaction among the neighboring V ions dominate up to 3% tensile strain along the  $b$ -axis, promoting AFM3 ordering. As expected, direct-exchange decreases with increasing distance between V ions along the  $b$ -direction, which is confirmed by declining magnitude of  $J_b$  [see Table S1<sup>59</sup>]. This is further substantiated by the DOS plots at various different tensile strain [Figure S11<sup>59</sup>]. Evidently, the bandwidth decreases with increasing tensile strain, which is a clear signature of decreasing overlap among atomic orbitals. As the distance between neighboring V ions increases further (along  $b$ -direction), for tensile strain of 4% and above, the direct-exchange becomes weaker than the halogen mediated superexchange interaction. As mentioned previously, since V-Cl-V bonds make an angle of  $\sim 90^\circ$ , a ferromagnetic superexchange interaction is possible among neighboring V ions, according to the Goodenough-Kanamori rules,<sup>66-68</sup> resulting in a positive value for  $J_b$  and FM ordering along the  $b$ -axis. Unlike  $J_b$ , the other two magnetic exchange coupling parameters,  $J_a$  and  $J_{ab}$  (the latter being always greater than

the former, see Table S1<sup>59</sup>) remain almost unchanged for a tensile strain along the  $b$ -axis. Since the possibility of oxygen mediated superexchange has already been ruled out, tensile strain along the  $a$ -direction has no effect on the magnetic ground state.

Based on the above discussion, evolution of the magnetic ground state as a function of strain can be summarized as following. For a tensile strain ranging from 0-3% (along  $b$ -direction, as well as biaxial), negative values of  $J_b$  results in anti-parallel spin alignment along the  $b$ -axis, while positive values of  $J_{ab}$  results in a parallel spin alignment for the diagonally located V ions [Figure 1(a) and 3(f)], yielding the AFM3 ground-state magnetic ordering. For 4% and higher strain percent (along  $b$ -direction, as well as biaxial), we obtain positive values for all the exchange coupling parameters, resulting in FM ground-state magnetic ordering. The transition from AFM3 to FM ground state takes place, because the sign of  $J_b$  flips [Figure 3(f)] as the Cl-mediated superexchange mechanism becomes dominant at tensile strain of 4% and above.

We already have discussed about the violation of the  $d^0$  rule in  $\text{VOCl}_2$  monolayer. In order to further check whether  $d$ -orbital occupancy has any role on the strain dependence of ferroelectric properties described so far, a  $\text{TiOCl}_2$  ferroelectric monolayer is chosen, which has a  $d^0$  configuration for the Ti ion; and polar displacement of the Ti ion (which is proportional to the spontaneous polarization) is calculated [Figure S12<sup>59</sup>]. Similar to the case of  $\text{VOCl}_2$  (V  $d^1$ ), polar displacement in  $\text{TiOCl}_2$  (Ti  $d^0$ ) monolayer also increases with uniaxial tensile strain along the polar axis ( $a$ -axis), as well as biaxial tensile strain but it remains unaffected by the tensile strain along the  $b$ -axis. This clearly proves that the enhancement in spontaneous electric polarization for tensile strain along the polar axis is independent of the  $d$ -orbital occupancy of the transition metal.

Interestingly, SOC is found to increase the equilibrium lattice parameter of  $\text{VOCl}_2$  by nearly 3% [Figure S13<sup>59</sup>]. However, even with SOC, AFM3 is found to be the ground state in equilibrium and it is transformed to a FM state at only  $\sim 2\%$  tensile strain [Figure S13<sup>59</sup>], while rest of the physics remain unchanged. A lower value of tensile strain can further increase the chance of realizing such a magnetic phase transition in an experimental set-up. In order to check the robustness of the magnetic

ground state, with the inclusion of Hubbard corrections for the localized  $d$ -electrons on V ions, DFT+U based calculations are carried out. A qualitatively similar magnetic phase transition from the AFM3 to FM state is observed under uni-axial strain along the  $b$ -axis and biaxial strain, for both vdW-DF2 functional [Figure S14<sup>59</sup>] and PBE functional [Figure S15<sup>59</sup>]. Similar to the case of SOC, magnitude of strain required for magnetic phase transition decreases with increasing value of  $U$ . Although the bandgap reduces due to the AFM3 to FM transition, the latter is still found to be in an insulating state, with its bandgap increasing further with tensile strain, which is more effective when applied along the polar  $a$ -axis, than that of non-polar  $b$ -axis [Figure S16<sup>59</sup>].

#### IV. CONCLUSIONS

In summary, we find  $\text{VOCl}_2$  to be a unique multiferroic monolayer, where tensile strain along the polar axis provides (a) high electric polarization, (b) increased ferroelectric stability and (c) enhanced insulating nature; while along the non-polar axis it causes a magnetic phase transition. Moreover, as the ferroelectricity and magnetism can be tuned independently via tensile strain along different in plane crystallographic directions, this material offers a unique opportunity to design 2D type-I multiferroic based nanoelectronic devices, having the flexibility to increase or decrease electric polarization without affecting the monolayer's magnetic properties, and vice-versa. We also find the tensile strain to be beneficial for the purpose of increasing ferroelectric and ferromagnetic Curie temperature of  $\text{VOCl}_2$  monolayer. Our work thus reveals the versatility of  $\text{VOCl}_2$ , attainable via strain engineering; and this is expected to encourage further theoretical and experimental study of the  $\text{VOX}_2$  family of monolayers to realize new multiferroic materials for low-dimensional technologies.

#### Acknowledgements

We acknowledge funding from SERB (EMR/2017/004970 and CRG/2018/002440). We also thank computer center IIT Kanpur for providing HPC facility.

\* amahajan@iitk.ac.in

† bsomnath@iitk.ac.in

<sup>1</sup> Hans Schmid, "Multi-ferroic magneto-electrics," *Ferroelectrics* **162**, 317–338 (1994), <https://doi.org/10.1080/00150199408245120>

<sup>2</sup> Daniel Khomskii, "Classifying multiferroics: Mechanisms and effects," *Physics* **20**, 1–8 (2009)

<sup>3</sup> N. A. Spaldin and R. Ramesh, "Advances in magnetoelectric multiferroics," *Nature Materials* **18**, 203–212 (2019)

<sup>4</sup> Nicola A. Spaldin and Manfred Fiebig, "The renaissance of magnetoelectric multiferroics," *Science* **309**, 391–392 (2005), <https://science.sciencemag.org/content/309/5733/391.full.pdf>

<sup>5</sup> Martin Gajek, Manuel Bibes, Stéphane Fusil, Karim Bouzehouane, Josep Fontcuberta, Agnès Barthélémy, and Albert Fert, "Tunnel junctions with multiferroic barriers," *Nature Materials* **6**, 296–302 (2007)

- <sup>6</sup> J. F. Scott, "Multiferroic memories," *Nature Materials* **6**, 256–257 (2007)
- <sup>7</sup> J. Wang, J. B. Neaton, H. Zheng, V. Nagarajan, S. B. Ogale, B. Liu, D. Viehland, V. Vaithyanathan, D. G. Schlom, U. V. Waghmare, N. A. Spaldin, K. M. Rabe, M. Wuttig, and R. Ramesh, "Epitaxial bifeo<sub>3</sub> multiferroic thin film heterostructures," *Science* **299**, 1719–1722 (2003), <https://science.sciencemag.org/content/299/5613/1719.full.pdf><sup>21</sup>
- <sup>8</sup> R. Ramesh and Nicola A. Spaldin, "Multiferroics: progress and prospects in thin films," *Nature Materials* **6**, 21–29 (2007)
- <sup>9</sup> Shuai Dong, Jun-Ming Liu, Sang-Wook Cheong, and Zhifeng Ren, "Multiferroic materials and magnetoelectric physics: symmetry, entanglement, excitation, and topology," *Advances in Physics* **64**, 519–626 (2015), <https://doi.org/10.1080/00018732.2015.1114338>
- <sup>10</sup> Jing Ma, Jiamian Hu, Zheng Li, and Ce-Wen Nan, "Recent progress in multiferroic magnetoelectric composites: from bulk to thin films," *Advanced Materials* **23**, 1062–1087 (2011), <https://onlinelibrary.wiley.com/doi/pdf/10.1002/adma.201003636>
- <sup>11</sup> Wenjun Ding, Jianbao Zhu, Zhe Wang, Yanfei Gao, Di Xiao, Yi Gu, Zhenyu Zhang, and Wenguang Zhu, "Prediction of intrinsic two-dimensional ferroelectrics in in<sub>2</sub>se<sub>3</sub> and other iii<sub>2</sub>-vi<sub>3</sub> van der waals materials," *Nature Communications* **8**, 14956 (2017)
- <sup>12</sup> Ruixiang Fei, Wei Kang, and Li Yang, "Ferroelectricity and phase transitions in monolayer group-iv monochalcogenides," *Phys. Rev. Lett.* **117**, 097601 (2016)
- <sup>13</sup> Kai Chang, Junwei Liu, Haicheng Lin, Na Wang, Kun Zhao, Anmin Zhang, Feng Jin, Yong Zhong, Xiaopeng Hu, Wenhui Duan, Qingming Zhang, Liang Fu, Qi-Kun Xue, Xi Chen, and Shuai-Hua Ji, "Discovery of robust in-plane ferroelectricity in atomic-thick sn<sub>2</sub>e," *Science* **353**, 274–278 (2016), <https://science.sciencemag.org/content/353/6296/274.full.pdf>
- <sup>14</sup> Dillon D. Fong, G. Brian Stephenson, Stephen K. Streiffer, Jeffrey A. Eastman, Orlando Auciello, Paul H. Fuoss, and Carol Thompson, "Ferroelectricity in ultrathin perovskite films," *Science* **304**, 1650–1653 (2004), <https://science.sciencemag.org/content/304/5677/1650.full.pdf><sup>27</sup>
- <sup>15</sup> Javier Junquera and Philippe Ghosez, "Critical thickness for ferroelectricity in perovskite ultrathin films," *Nature* **422**, 506–509 (2003)
- <sup>16</sup> M. Dawber, K. M. Rabe, and J. F. Scott, "Physics of thin-film ferroelectric oxides," *Rev. Mod. Phys.* **77**, 1083–1130 (2005)
- <sup>17</sup> Yandong Ma, Ying Dai, Meng Guo, Chengwang Niu, Yingtao Zhu, and Baibiao Huang, "Evidence of the existence of magnetism in pristine vx<sub>2</sub> monolayers (x = s, se) and their strain-induced tunable magnetic properties," *ACS Nano* **6**, 1695–1701 (2012), pMID: 22264067, <https://doi.org/10.1021/nn204667z>
- <sup>18</sup> Hemant Kumar, Nathan C. Frey, Liang Dong, Babak Anasori, Yury Gogotsi, and Vivek B. Shenoy, "Tunable magnetism and transport properties in nitride mxenes," *ACS Nano* **11**, 7648–7655 (2017), pMID: 28558192, <https://doi.org/10.1021/acsnano.7b02578>
- <sup>19</sup> Qisheng Wu, Yehui Zhang, Qionghua Zhou, Jinlan Wang, and Xiao Cheng Zeng, "Transition-metal dihydride monolayers: A new family of two-dimensional ferromagnetic materials with intrinsic room-temperature half-metallicity," *The Journal of Physical Chemistry Letters* **9**, 4260–4266 (2018), pMID: 30001619, <https://doi.org/10.1021/acs.jpcclett.8b01976>
- <sup>20</sup> Chengxi Huang, Junsheng Feng, Fang Wu, Dildar Ahmed, Bing Huang, Hongjun Xiang, Kaiming Deng, and Erjun Kan, "Toward intrinsic room-temperature ferromagnetism in two-dimensional semiconductors," *Journal of the American Chemical Society* **140**, 11519–11525 (2018), pMID: 30130098, <https://doi.org/10.1021/jacs.8b07879>
- <sup>21</sup> Naihua Miao, Bin Xu, Linggang Zhu, Jian Zhou, and Zhimei Sun, "2d intrinsic ferromagnets from van der waals antiferromagnets," *Journal of the American Chemical Society* **140**, 2417–2420 (2018), pMID: 29400056, <https://doi.org/10.1021/jacs.7b12976>
- <sup>22</sup> Lei Li and Menghao Wu, "Binary compound bilayer and multilayer with vertical polarizations: Two-dimensional ferroelectrics, multiferroics, and nanogenerators," *ACS Nano* **11**, 6382–6388 (2017), pMID: 28602074, <https://doi.org/10.1021/acsnano.7b02756>
- <sup>23</sup> Menghao Wu, Shuai Dong, Kailun Yao, Junming Liu, and Xiao Cheng Zeng, "Ferroelectricity in covalently functionalized two-dimensional materials: Integration of high-mobility semiconductors and nonvolatile memory," *Nano Letters* **16**, 7309–7315 (2016), pMID: 27740764, <https://doi.org/10.1021/acs.nanolett.6b04309>
- <sup>24</sup> Anand Chandrasekaran, Avanish Mishra, and Abhishek Kumar Singh, "Ferroelectricity, antiferroelectricity, and ultrathin 2d electron/hole gas in multifunctional monolayer mxene," *Nano Letters* **17**, 3290–3296 (2017), pMID: 28375621, <https://doi.org/10.1021/acs.nanolett.7b01035>
- <sup>25</sup> Xiao Tang and Liangzhi Kou, "Two-dimensional ferroics and multiferroics: Platforms for new physics and applications," *The Journal of Physical Chemistry Letters* **10**, 6634–6649 (2019), pMID: 31600077, <https://doi.org/10.1021/acs.jpcclett.9b01969>
- <sup>26</sup> Qing Yang, Wei Xiong, Lin Zhu, Guoying Gao, and Menghao Wu, "Chemically functionalized phosphorene: Two-dimensional multiferroics with vertical polarization and mobile magnetism," *Journal of the American Chemical Society* **139**, 11506–11512 (2017), pMID: 28745054, <https://doi.org/10.1021/jacs.7b04422>
- <sup>27</sup> Zhengyuan Tu, Menghao Wu, and Xiao Cheng Zeng, "Two-dimensional metal-free organic multiferroic material for design of multifunctional integrated circuits," *The Journal of Physical Chemistry Letters* **8**, 1973–1978 (2017), pMID: 28412811, <https://doi.org/10.1021/acs.jpcclett.7b00636>
- <sup>28</sup> Chengxi Huang, Yongping Du, Haiping Wu, Hongjun Xiang, Kaiming Deng, and Erjun Kan, "Prediction of intrinsic ferromagnetic ferroelectricity in a transition-metal halide monolayer," *Phys. Rev. Lett.* **120**, 147601 (2018)
- <sup>29</sup> Yinghe Zhao, Lingfang Lin, Qionghua Zhou, Yunhai Li, Shijun Yuan, Qian Chen, Shuai Dong, and Jinlan Wang, "Surface vacancy-induced switchable electric polarization and enhanced ferromagnetism in monolayer metal trihalides," *Nano Letters* **18**, 2943–2949 (2018), pMID: 29668292, <https://doi.org/10.1021/acs.nanolett.8b00314>
- <sup>30</sup> Xiangyang Li, Xingxing Li, and Jinlong Yang, "Two-dimensional multifunctional metal-organic frameworks with simultaneous ferro-/ferrimagnetism and vertical ferroelectricity," *The Journal of Physical Chemistry Letters* **11**, 4193–4197 (2020), pMID: 32370503, <https://doi.org/10.1021/acs.jpcclett.0c01033>
- <sup>31</sup> Xukun Feng, Jian Liu, Xikui Ma, and Mingwen Zhao, "Ferroelectricity and multiferroicity in two-dimensional



- sc2p2se6 and sccrp2se6 monolayers,” *Phys. Chem. Chem. Phys.* **22**, 7489–7496 (2020)
- <sup>32</sup> Wei Luo, Ke Xu, and Hongjun Xiang, “Two-dimensional hyperferroelectric metals: A different route to ferromagnetic-ferroelectric multiferroics,” *Phys. Rev. B* **96**, 235415 (2017)
  - <sup>33</sup> Jingshan Qi, Hua Wang, Xiaofang Chen, and Xiaofeng Qian, “Two-dimensional multiferroic semiconductors with coexisting ferroelectricity and ferromagnetism,” *Applied Physics Letters* **113**, 043102 (2018), <https://doi.org/10.1063/1.5038037>
  - <sup>34</sup> Bao-Wen Li, Minoru Osada, Yasuo Ebina, Shigenori Ueda, and Takayoshi Sasaki, “Coexistence of magnetic order and ferroelectricity at 2d nanosheet interfaces,” *Journal of the American Chemical Society* **138**, 7621–7625 (2016), pMID: 27295544, <https://doi.org/10.1021/jacs.6b02722>
  - <sup>35</sup> Jun-Jie Zhang, Lingfang Lin, Yang Zhang, Menghao Wu, Boris I. Yakobson, and Shuai Dong, “Type-II multiferroic hf2vc2f2 mxene monolayer with high transition temperature,” *Journal of the American Chemical Society* **140**, 9768–9773 (2018), pMID: 29992814, <https://doi.org/10.1021/jacs.8b06475>
  - <sup>36</sup> Haoqiang Ai, Xiaohan Song, Siyun Qi, Weifeng Li, and Mingwen Zhao, “Intrinsic multiferroicity in two-dimensional vocl2 monolayers,” *Nanoscale* **11**, 1103–1110 (2019)
  - <sup>37</sup> Hengxin Tan, Menglei Li, Haitao Liu, Zhirong Liu, Yuanchang Li, and Wenhui Duan, “Two-dimensional ferromagnetic-ferroelectric multiferroics in violation of the  $d^0$  rule,” *Phys. Rev. B* **99**, 195434 (2019)
  - <sup>38</sup> Nicola A. Hill, “Why are there so few magnetic ferroelectrics?” *The Journal of Physical Chemistry B* **104**, 6694–6709 (2000), <https://doi.org/10.1021/jp000114x>
  - <sup>39</sup> Hua Wang and Xiaofeng Qian, “Two-dimensional multiferroics in monolayer group IV monochalcogenides,” *2D Materials* **4**, 015042 (2017)
  - <sup>40</sup> Shiyang Shen, Chang Liu, Yandong Ma, Baibiao Huang, and Ying Dai, “Robust two-dimensional ferroelectricity in single-layer  $\gamma$ -sbp and  $\gamma$ -sbas,” *Nanoscale* **11**, 11864–11871 (2019)
  - <sup>41</sup> W. Kohn and L. J. Sham, “Self-consistent equations including exchange and correlation effects,” *Phys. Rev.* **140**, A1133–A1138 (1965)
  - <sup>42</sup> G. Kresse and J. Furthmüller, “Efficiency of ab-initio total energy calculations for metals and semiconductors using a plane-wave basis set,” *Computational Materials Science* **6**, 15 – 50 (1996)
  - <sup>43</sup> G. Kresse and J. Furthmüller, “Efficient iterative schemes for ab initio total-energy calculations using a plane-wave basis set,” *Phys. Rev. B* **54**, 11169–11186 (1996)
  - <sup>44</sup> P. E. Blöchl, “Projector augmented-wave method,” *Phys. Rev. B* **50**, 17953–17979 (1994)
  - <sup>45</sup> G. Kresse and D. Joubert, “From ultrasoft pseudopotentials to the projector augmented-wave method,” *Phys. Rev. B* **59**, 1758–1775 (1999)
  - <sup>46</sup> John P. Perdew, Kieron Burke, and Matthias Ernzerhof, “Generalized gradient approximation made simple,” *Phys. Rev. Lett.* **77**, 3865–3868 (1996)
  - <sup>47</sup> M. Dion, H. Rydberg, E. Schröder, D. C. Langreth, and B. I. Lundqvist, “Van der waals density functional for general geometries,” *Phys. Rev. Lett.* **92**, 246401 (2004)
  - <sup>48</sup> Guillermo Román-Pérez and José M. Soler, “Efficient implementation of a van der waals density functional: Application to double-wall carbon nanotubes,” *Phys. Rev. Lett.* **103**, 096102 (2009)
  - <sup>49</sup> Kyuho Lee, Éamonn D. Murray, Lingzhu Kong, Bengt I. Lundqvist, and David C. Langreth, “Higher-accuracy van der waals density functional,” *Phys. Rev. B* **82**, 081101 (2010)
  - <sup>50</sup> Jiří Klimeš, David R. Bowler, and Angelos Michaelides, “Van der waals density functionals applied to solids,” *Phys. Rev. B* **83**, 195131 (2011)
  - <sup>51</sup> S. L. Dudarev, G. A. Botton, S. Y. Savrasov, C. J. Humphreys, and A. P. Sutton, “Electron-energy-loss spectra and the structural stability of nickel oxide: An lsd+u study,” *Phys. Rev. B* **57**, 1505–1509 (1998)
  - <sup>52</sup> <https://www.ccdc.cam.ac.uk/structures/Home/>, “Link to the inorganic crystal structure database (icsd).”
  - <sup>53</sup> Xavier Gonze and Changyol Lee, “Dynamical matrices, born effective charges, dielectric permittivity tensors, and interatomic force constants from density-functional perturbation theory,” *Phys. Rev. B* **55**, 10355–10368 (1997)
  - <sup>54</sup> R. D. King-Smith and David Vanderbilt, “Theory of polarization of crystalline solids,” *Phys. Rev. B* **47**, 1651–1654 (1993)
  - <sup>55</sup> Raffaele Resta, “Macroscopic polarization in crystalline dielectrics: the geometric phase approach,” *Rev. Mod. Phys.* **66**, 899–915 (1994)
  - <sup>56</sup> Ankit Izard and Claude Ederer, “Interplay between chemical order and magnetic properties in  $\text{Li}_0$  feni (tetraenaite): A first-principles study,” *Phys. Rev. Materials* **4**, 054418 (2020)
  - <sup>57</sup> A.I. Liechtenstein, M.I. Katsnelson, V.P. Antropov, and V.A. Gubanov, “Local spin density functional approach to the theory of exchange interactions in ferromagnetic metals and alloys,” *Journal of Magnetism and Magnetic Materials* **67**, 65 – 74 (1987)
  - <sup>58</sup> G. H. O. Daalderop, P. J. Kelly, and M. F. H. Schuurmans, “Magnetocrystalline anisotropy and orbital moments in transition-metal compounds,” *Phys. Rev. B* **44**, 12054–12057 (1991)
  - <sup>59</sup> “See supplemental material for: Schematic representation of crystal structure of vocl2 monolayer; magnetic orderings considered in this work; dependency of polarization on polar displacement; phonon spectra to determine stability of fe-fm vocl2 monolayers; schematic representation of ferroelectric switching pathway via afe intermediate state; effect of uniaxial tensile strain along in-plane lattice vectors on the ferroelectric switching energy barriers; effect of uniaxial tensile strain along in-plane lattice vectors on the exchange coupling parameter along  $b$ -axis; orbital-resolved density of states plots (zero strain); schematic representation of exchange interactions between  $v$ - $d$  electrons; orbital-resolved density of states plots (non-zero tensile strain); polar displacement in tiocl2 monolayer with strain; effect of soc, vdw-df2+u and pbe+u on the energy difference between strained structures; variation of band gap with strain; values of exchange coupling parameters; values of mae varying with strain; structural parameters for vocl2 monolayer under different exchange and correlation functionals.”
  - <sup>60</sup> P. A. Fleury, J. F. Scott, and J. M. Worlock, “Soft phonon modes and the 110°k phase transition in  $\text{srTiO}_3$ ,” *Phys. Rev. Lett.* **21**, 16–19 (1968)
  - <sup>61</sup> Yubo Zhang, Jianwei Sun, John P. Perdew, and Xifan Wu, “Comparative first-principles studies of prototypical ferroelectric materials by lda, gga, and scan meta-gga,” *Phys. Rev. B* **96**, 035143 (2017)

- <sup>62</sup> Meng Ye and David Vanderbilt, “Ferroelectricity in corundum derivatives,” *Phys. Rev. B* **93**, 134303 (2016)
- <sup>63</sup> N. D. Mermin and H. Wagner, “Absence of ferromagnetism or antiferromagnetism in one- or two-dimensional isotropic heisenberg models,” *Phys. Rev. Lett.* **17**, 1133–1136 (1966)
- <sup>64</sup> Yingjie Sun, Zhiwen Zhuo, Xiaojun Wu, and Jinlong Yang, “Room-temperature ferromagnetism in two-dimensional fe<sub>2</sub>si nanosheet with enhanced spin-polarization ratio,” *Nano Letters* **17**, 2771–2777 (2017), pMID: 28441496, <https://doi.org/10.1021/acs.nanolett.6b04884>
- <sup>65</sup> Bevin Huang, Genevieve Clark, Efrén Navarro-Moratalla, Dahlia R. Klein, Ran Cheng, Kyle L. Seyler, Ding Zhong, Emma Schmidgall, Michael A. McGuire, David H. Cobden, Wang Yao, Di Xiao, Pablo Jarillo-Herrero, and Xiaodong Xu, “Layer-dependent ferromagnetism in a van der waals crystal down to the monolayer limit,” *Nature* **546**, 270–273 (2017)
- <sup>66</sup> John B. Goodenough, “Theory of the role of covalence in the perovskite-type manganites [La, *m*(II)]MnO<sub>3</sub>,” *Phys. Rev.* **100**, 564–573 (1955)
- <sup>67</sup> John B. Goodenough, “An interpretation of the magnetic properties of the perovskite-type mixed crystals la<sub>1-x</sub>srxcoo<sub>3-λ</sub>,” *Journal of Physics and Chemistry of Solids* **6**, 287 – 297 (1958)
- <sup>68</sup> Junjiro Kanamori, “Superexchange interaction and symmetry properties of electron orbitals,” *Journal of Physics and Chemistry of Solids* **10**, 87 – 98 (1959)